www.czasopisma.pan.pl PAN POLSKA AKADEMIA NAUK www.journals.pan.pl

Arch. Min. Sci. **69** (2024), 4, 685-709

Electronic version (in color) of this paper is available: http://mining.archives.pl

DOI: https://doi.org/10.24425/ams.2024.152580

JACEK JAKUBOWSKI[1*], TUAN ANH PHAN[2]

DISTINCT ELEMENT SIMULATION OF ROCK MASS DEFORMATION NEAR TUNNELS IN COMPLEX GEOLOGICAL CONDITIONS, GUIDED BY STATISTICAL EXPERIMENTAL DESIGN

The mechanics of a flysch rock mass is determined by its complex discontinuity, heterogeneity, anisotropy, and diverse deformation modes. This study proposes a new methodology to simulate the deformation of Carpathian flysch in the vicinity of tunnels, employing the distinct element method (DEM), global-local modelling approach and a hybrid representation of discontinuities. The methodology enables the simulation of a wide range of structural models and properties of Carpathian flysch and reduces the computational complexity of numerical models. A global model reflects the initial stress field. Local models detail the properties of joint sets separating rock blocks and the properties of the ubiquitous joint model material inside the discrete blocks. Both direct and indirect representations of discontinuities contribute to the model response. The numerical model is addressed as a multiparameter system and examined through statistical design of experiments (DOE). The model is calibrated and validated using field measurements of displacements and convergences. The factors contributing to uncertainty in the simulation results are considered. A parametric analysis was conducted on the deformation of flysch rock mass surrounding a tunnel, evaluating the impact of bedding orientation, depth, and support stiffness. Bedding dip direction explained the asymmetry in sidewall convergence and its changes. Discontinuity stiffness and dilation, rarely studied model parameters, were found to have a significant effect on simulation error.

Keywords: Jointed rock mass; flysch; tunnel; 3DEC; deformation; numerical simulation

1. Introduction

3DEC, developed by Itasca, is an advanced, three-dimensional implementation of the distinct element method (DEM) and represents a discontinuous rock mass as a collection of polyhedral

[1] DEPARTMENT OF CIVIL & GEOTECHNICAL ENGINEERING AND GEOMECHANICS, AGH UNIVERSITY OF KRAKOW, POLAND
[2] DEPARTMENT OF UNDERGROUND AND MINING CONSTRUCTION, HANOI UNIVERSITY OF MINNING AND GEOLOGY, VIETNAM

* Corresponding author email: jakubjac@agh.edu.pl

blocks [1,2]. Its application includes simulation of the behaviour of rock masses near tunnels and underground chambers [3-12], slopes and landslides [13-20], and mining excavations [21-26]. Jakubowski [27] proposed a methodology for the stochastic simulation of the stability of blocky structures around tunnels and chambers using 3DEC and the Monte Carlo scheme. The results were presented with the unstable area probability maps [28-30].

The global–local simulation approach involves using two models of different sizes (global and local models) to simulate the behaviour of the rock mass. Specifically, the large global model estimates the initial stress or strain field, which is subsequently used to reflect the boundary conditions of the small local model [22,31-33].

Numerical simulations of rock mass mechanics often involve complex model geometries, including multiple joints, detailed discretisation, and physical and geometrical nonlinearities. These simulations are time consuming, and the number of numerical experiments is highly limited. Experimental design (DOE) represents an important group of statistical methods primarily used for the design and analysis of laboratory and field experiments; however, these methods are equally beneficial for the design of numerical experiments, providing a feasibly small number of simulations and strong statistical inference. In the field of rock mechanics and tunnelling, DOE is mostly used for screening factors or optimal selection of model parameter values [34-40].

The Carpathian flysch is a complex heterogeneous rock mass consisting of sandstone, shale, and siltstone in varying proportions. It is characterised by the presence of bedding and joint sets, anisotropy due to bedding, anisotropy in the rock material, and significant spatial variation in the orientation and density of discontinuities. Under these circumstances, analytical design methods are insufficient or require confirmation; therefore, supporting numerical simulations are welcome. Classical continuous-domain numerical methods do not realistically represent the discontinuous displacement field, interactions between discontinuities in flysch rock masses, or interactions between blocks. They cannot identify large deformations, translations, or rotations of blocks, which determine the displacement field and stability, in a tunnel. Moreover, they do not recognize contact and loss of contact between blocks. Methods based on rock wedge stability and block theory can be applied only to rock masses with a blocky structure. The structure of a flysch rock mass is diverse, and when the rock mass is heavily fractured, the assumptions made by the blocky methods are not satisfied. Heavy fracturing and blocky structures, both of which are characteristics of flysch rock masses, should be simulated within a single computational framework. DEM simulations could be a solution but only when 3D analysis is applied because of the significant influence of the orientations of the discontinuities on the rock mass behaviour. This requires large-scale 3D models that accurately reflect the initial stress field, boundary conditions, and dense discontinuity sets that form numerous small blocks. Meeting these criteria requires significant computational complexity and long computation times, resulting in the limited usability of classical DEM solutions for tunnel design practice.

This study presents a new pragmatic methodology for the numerical 3D simulation of the behaviour of flysch rock masses based on the discrete block approach and hybrid representation of joints. The numerical models have reduced computational complexity and can be used in parametric multivariate analyses, which are particularly useful for the design and monitoring of tunnel construction. The numerical model is regarded as a multiparameter system, and subject to mixed, D-optimal design experiments. The design analysis allows model examination through factor effects assessment, response-surface estimation, and analysis of variance. The methodology also incorporates uncertainty discussion, calibration, and validation of the models on the basis of in situ measurements.

2. Characteristics of hydrotechnical tunnels in Swinna Poreba

The Carpathians are among the youngest mountain ranges in Europe. The Carpathians include the Outer Carpathians, which contain Cretaceous and Tertiary flysch sediments. Flysch rock masses are heterogeneous, discontinuous, and anisotropic [41-57]. The tunnels in Swinna Poreba are located in the northern part of the Silesian and Lesser Beskids, within the Carpathian flysch rocks, in a series of layers consisting of alternating sandstone and shale layers. A characteristic feature of this sandstone and shale complex is the variability in bed thickness, ranging from thin to thick beds. The proportion of sandstone varies from 85% to 40%. Thinly layered sandstone contains significant amounts of mica, feldspar, and fine organic fractions. Shales are typically grey or black and contain clays and mudstones.

There are three types of discontinuities in the area: (1) bedding planes that separate layers; (2) joints that cut across to the bedding planes, arranged in two sets and oriented approximately perpendicular to the layers; and (3) dense and irregular schistosity that is parallel to the bedding. Tectonic disturbances include longitudinal and transverse displacements and fault zones 30-70 m in width. Landslides were identified near the entrances of the tunnels. The tunnel area encompasses rocks classified as geotechnical classes III, IV, and V according to the KF rock mass classification for Carpathian flysch [41].

The earth dam in Swinna Poreba is situated approximately 50 km southwest of Kraków, Poland. With the construction of the dam, a reservoir of approximately 1035 ha was created to supply water to the Silesian agglomeration, mitigate flood risk, and generate electricity. Two discharge and intake tunnels were constructed adjacent to the dam. These tunnels have inner diameters of 8.5-9 m. Their axes are shaped like arches with a total length of 625 m. They were excavated at an average depth of 55 m. The distance between the tunnel axes is 30 m (Fig. 1). A discharge tunnel is used to divert water below the dam. Three pipelines are located in the intake tunnel to power the turbines and deliver water to the water supply system.

The tunnels in Swinna Poreba were excavated using a blasting method similar to the New Austrian Tunnelling Method. The tunnelling process was divided into two stages. In the first stage, the upper parts of the tunnels (calottes) were constructed, and a primary support was established along the entire tunnel length. In the second stage, the lower parts of the tunnels were constructed, and the final reinforced concrete support was established. This study considered the measurements and models of the tunnels constructed in the first stage, that is, the tunnels with primary support.

The primary supports in the tunnels consist of steel rock bolts set in cement mortar, a layer of shotcrete with a mesh, and steel arches. The support properties were adjusted, depending on the geological conditions in the tunnel segments. The surveyed cross-sections were located at different locations with diverse geotechnical conditions, differing in overburden thickness, rock mass quality, and bedding orientation with respect to the tunnel axis. The support was established on the roof and sidewalls, and no invert bar was established at the bottom.

The reinforcement scheme involves 16 rock bolts in a cross-section with an axial spacing of 1 m. The rock bolts have a length of 3 m, a diameter of 22 mm, and capacity of 118 kN. V29 steel arches were used in the tunnels. The shotcrete support is approximately 20 cm thick and includes a mesh (Novomag). The linear elasticity modulus of the applied shotcrete is 23 GPa, and the Poisson's ratio is 0.2 [43].

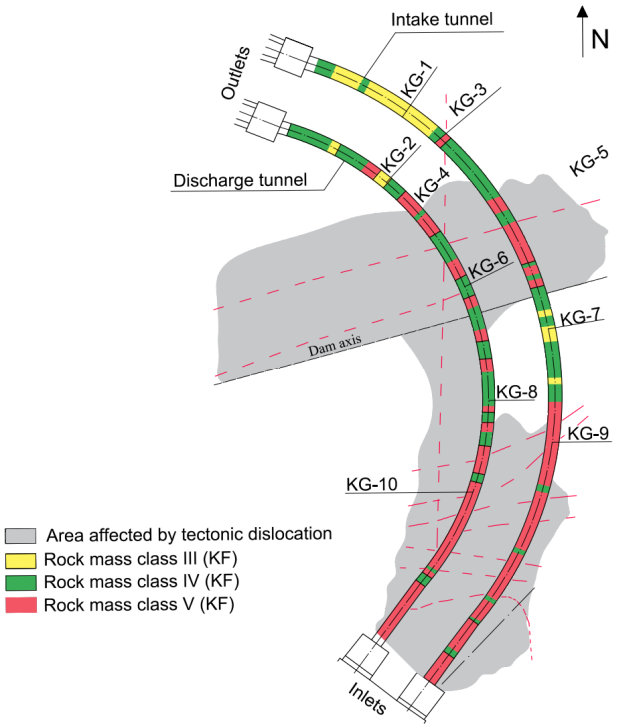

Fig. 1. Schematic of the hydrotechnical tunnels near the Swinna Poreba dam.
Based on Dynowska [44]. The rock mass quality corresponds to the KF classification [41]

3. Displacement and convergence measurements

The deformation of a rock mass near a tunnel is a visible effect of stress redistribution occurring within the rock mass and the interaction between the support and rock mass. During tunnel construction, deformation measurements are crucial for assessing the current condition, revealing the mechanical behaviour of the rock mass, and providing evidence for modifying the support or excavation method.

Deformation measurements performed during the first stage of tunnelling in Swinna Poreba include the vertical displacement of the surface above the tunnel axis (u_{sur}), vertical displacement of the tunnel roof (u_{roof}), horizontal convergence of the tunnel (k_1), left sidewall convergence (k_2), and right sidewall convergence (k_3). Convergence and displacement stabilisation occurred after approximately three months. Data from measurements of the stabilised displacements of the roof, surface and convergences were reported by Zabuski [43] and Dynowska [44], along with information on the technological and geotechnical disturbances that occurred during these measurements.

Geodetic survey benchmarks were embedded in the excavations as the tunnel advanced, where heavy equipment was moved, and where interruptions in the continuity of work were noted. Certain measurements in the tunnel segments passing below landslides and through faults were reported to be disturbed. The reported records of technological and geotechnical disturbances were confirmed via outlier analysis. Data disturbances were identified for the KG1, KG2, KG7,

KG9, and KG10 cross-sections. The cross-sections KG3, KG4, KG5, KG6, and KG8 did not contain disturbed data, and their characteristics were based solely on the original measurements. These five cross-sections were subsequently used for model validation.

The disturbed measurements that were identified were treated as missing data and replaced with approximations via the multidimensional k-nearest neighbour method. This method assigns values in place of missing data by measuring the distances between cases in a multidimensional space of variables. The procedure yielded the results presented in TABLE 1. This dataset forms the basis for investigating the numerical models.

TABLE 1

Deformation measurements in the cross-sections: vertical displacements of the roof and surface and three convergences. Data corrected via the *k*-nearest neighbour estimates are marked in grey. Negative displacement and convergence values indicate subsidence and distance reduction

Cross-Section	u_{roof} [mm]	u_{sur} [mm]	k_1 [mm]	k_2 [mm]	k_2 [mm]
KG1	−6.33	−4.56	−14.06	0.48	−10.03
KG2	−10.34	−3.67	−6.19	−3.74	−6.43
KG3	−6.20	−4.85	−10.14	0.42	−5.58
KG4	−6.45	−6.05	−4.37	2.59	−2.51
KG5	−11.40	−14.75	−19.82	−3.96	−7.96
KG6	−7.58	−12.64	−10.68	−3.13	−4.52
KG7	−16.30	−13.91	−11.03	−5.29	−10.04
KG8	−14.47	−13.06	−2.23	−3.21	−4.77
KG9	−7.70	−8.75	−19.06	−1.82	−5.05
KG10	−6.33	−5.45	−16.85	−7.01	−7.68

4. Simulation methodology

4.1. Elements and stages

The methodology of this study involved the integration of two models, global and local, with different scopes and levels of geometric representation (Fig. 2).

The global model was constructed primarily to determine the initial local stress field around the measurement cross-sections before tunnelling. The initial stress field and static boundary conditions were then assigned to the local models. The local models and discontinuity geometry offer greater detail on each of the ten cross-sections examined, based on the characteristics of the rock mass. These models describe the fracture network, fracture characteristics, and properties of the rocks and rock masses. Loads, including the initial stress field and boundary conditions, were derived from the global model and support properties, respectively, for each of the ten local models.

In the global model, the anisotropy of a flysch rock mass was approximated by the properties of a transversely isotropic continuous medium. In the local model, the anisotropy of the rock mass was represented by three sets of discontinuities and the anisotropy of the material inside the ubiquitous joint blocks.

During the simulation, the diversity in the support and geological conditions in the different tunnel sections was considered, as was the gradual unloading of the tunnel contour due to the delay between face advance and support installation.

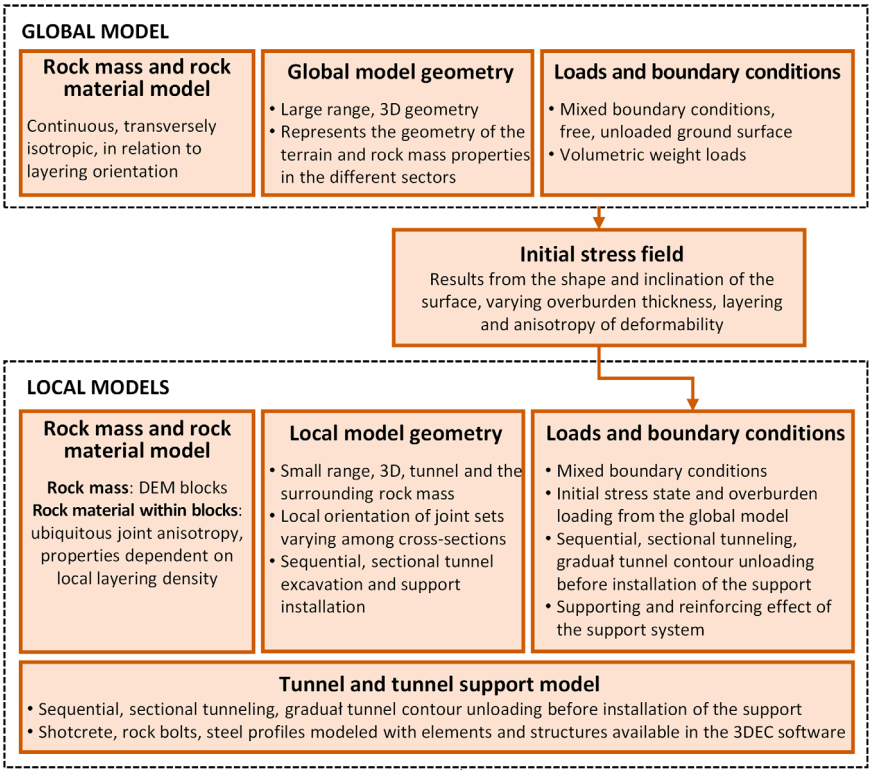

Fig. 2. Elements of the global and local models

The applied methodology encompasses several stages of modelling, simulation, and analysis, as shown in Fig. 3. It starts with the construction of a global model and local base series of models. The parameters of these models are derived from the documented geotechnical conditions in the Swinna Poreba area. The proposed methodology includes examining the base model by analysing the influence of environmental factors and calibrating the model. The next step is model validation using in situ measurements. The validated model can then be used to simulate various tunnel design variants.

4.2. Geometry, boundary conditions, and loads

The geometry of the global model, which depicts the terrain surface and tunnels, is shown in Fig. 4. The modelled area was 400 m long and 400 m wide. Following the principles of optimal 3DEC model construction, the model was divided into 28,060 blocks and 1,613,747 finite-difference discretisation zones. In the global model, kinematic boundary conditions were applied to five walls. The upper surface was free. The rock mass in the global model was represented as a transversely isotropic domain.

The global 3DEC model describes the geometry of a large area, the slope geometry, and the varying depths of the tunnel axis. The local models (Fig. 5) provide a detailed local representa-

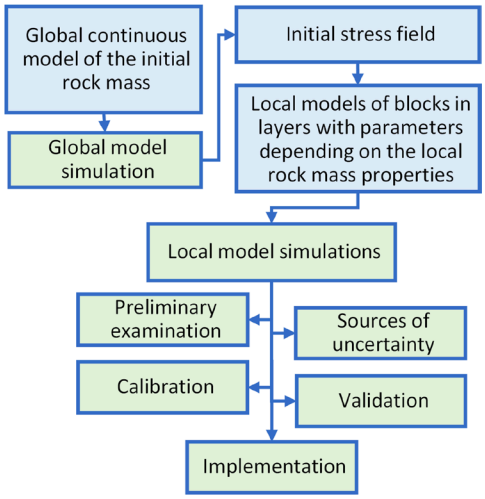

Fig. 3. Stages of the proposed methodology

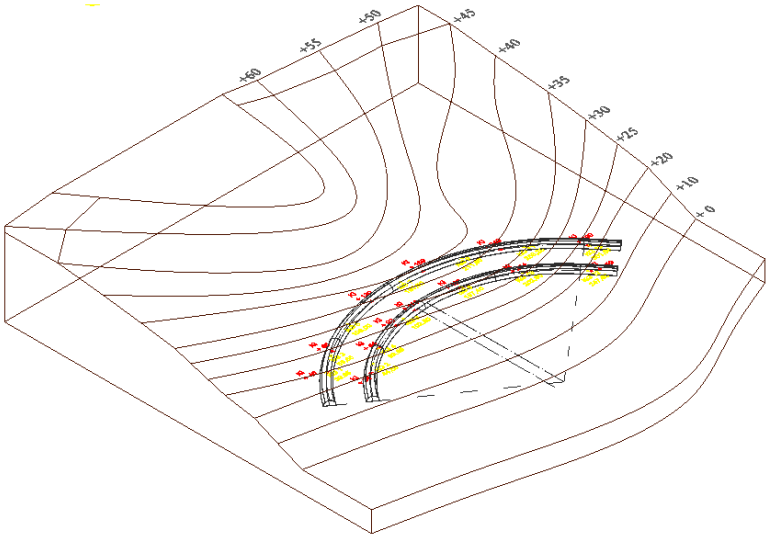

Fig. 4. Global model topography and tunnels

tion of the rock mass near the tunnels in terms of excavation geometry, support, and properties. Ten local models were created for the cross-sections where survey benchmarks were installed: five for the intake tunnel and five for the discharge tunnel.

The inclination and orientation of a discontinuity concerning the tunnel axis, the density of discontinuities, the thickness of the overburden, and tunnel support vary in the sections along the tunnel axis; these factors are directly or indirectly (through boundary conditions and the original stress field) reproduced by the local models. The models have an external cuboid geometry, and

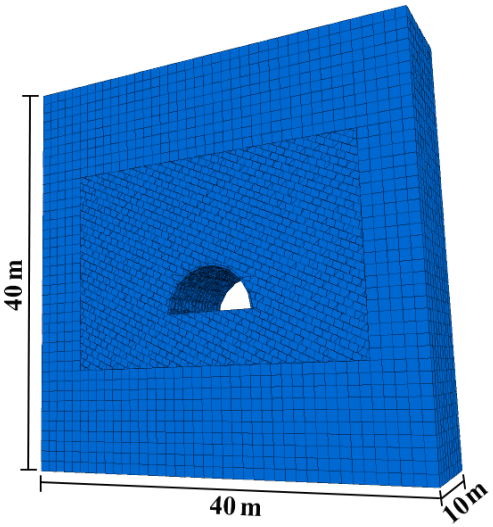

Fig. 5. Local model geometry

the internal geometry is determined by the tunnel, supports, and discontinuity networks around the tunnel (bedding planes and two sets of joints). In this model, the bedding planes and joints are represented by first-order (persistent) and second-order discontinuities, respectively.

Kinematic boundary conditions were applied perpendicularly to the five walls of the model. Static conditions were set on the upper wall to reflect the overburden pressure transferred from the global model. Additionally, the initial stress field inherited from the global model was replicated. The stress field transfer operation from the global model to the local model was performed using the 3DEC scripting language.

The tunnel support consists of rock bolts, shotcrete reinforced with steel mesh, and steel arches. The local rock bolt model strengthens the rock mass representation, with tangential and normal reaction forces acting in response to relative block displacements along the discontinuities. The implementation and properties of the rock bolt model are described in detail in the 3DEC software documentation [2]. The rock bolt support in the Swinna Poreba tunnels and the models comprises 16 rock bolts in a row with a 1 m spacing between rows. In the proposed approach, the concrete support is represented by 3DEC blocks, and the steel arches are represented by plate structural elements, which are used to simulate the support through matrix structural analysis. The thickness of the shotcrete layer was 0.2 m. The spacing between steel arches varied from 0.5 m to 1.0 m in the different cross-sections. In some tunnel segments, no steel arches were installed. Consequently, the models for the respective cross-sections also lack arches. The model reproduces the sequence of contour unloading, deformation, and delayed support and survey benchmark installation.

4.3. Rock material properties and bedding plane spacing

Discontinuity spacing affects the size of rock blocks and the displacement and deformation of the rock mass around a tunnel. The available information and direct measurements from

geological mapping were utilised in this study to calculate bedding plane spacing for the computational model.

The study area is dominated by alternating layers of sandstones and shales. The spacing of the bedding planes introduced into the model was determined on the basis of the average thickness of the shale and sandstone layers, as well as the percentage composition of the shales and sandstones in the rock mass, as a weighted average of the layer spacing in the rock mass.

According to the adopted jointed rock mass model, for actual bedding plane spacings (m_r) greater than or equal to the minimum equivalent spacing in the model (m_{eq} = 0.724 m), the spacing reflected in the model is equal to the actual spacing. For small actual spacings, the modelled spacing equals m_{equi}, and the ubiquitous joint blocks represent the behaviour of a dense network of discontinuities. The properties of these blocks depend on the actual discontinuity spacing.

In the local model, the strength properties of the ubiquitous joints inside the rock blocks were dependent on the properties of the actual rock material, the properties of the discontinuities, and the average normal spacing of the bedding planes.

Based on the study by Zabuski [43], the parameters of the actual rock material in the tunnel area were assigned as follows: rock cohesion c_{rock} = 0.135 MPa, discontinuity cohesion c_{joint} = 0.011 MPa, internal friction angle of rocks φ_{rock} = 30°, friction angle of discontinuities φ_{joint} = 10.2°, and uniaxial tensile strength of rocks $\sigma_{r|rock}$ = 0.067 MPa.

The shear strength of the discontinuities was assumed to be proportional to their average normal spacing. Proportional reductions in strength, cohesion, and the tangent of the friction angle were also assumed. Therefore, the tangents of the friction angle and cohesion are proportional to the average normal spacing of the discontinuities in the cross-section (m_r). For a bedding plane spacing equal to the equivalent material spacing (m_{eq} = 0.724 m), the strength is equal to that of the rock material. For a spacing that is hypothetically equal to zero, the strength is equal to that of a bedding plane discontinuity.

Based on this rule, the strength properties of the equivalent rock material c_{eq}, φ_{eq} and $\sigma_{r|eq}$ were calculated as functions of m_r, c_{joint}, c_{rock}, φ_{joint}, and φ_{rock}.

In all the sections considered, the actual discontinuity spacing was less than the spacing assumed for the equivalent rock material. If $m_r < m_{eq}$, the above equations are applied: for $m_r \geq m_{eq}$, $m_{zast} = m_r$ should be considered, implying that the modelled discontinuity spacing equals the actual spacing and that the properties of the equivalent rock material are the same as those of the actual rock material. The tangent of the dilation angle was assumed to be half of the tangent of the friction angle.

5. Simulation results for the Swinna Poreba tunnels

5.1. Summary of the parameters

The parameters of the base series of models are derived from geological documentation and studies on the rock mass properties and technology of tunnelling in Swinna Poreba [42-44]. The base series of local models includes ten cross-section models (KG1-KG10) with different rock masses and support parameters in these locations (TABLES 2 and 3 and Fig. 6). Therefore, the ten local models in the base series were built using the same rules and methods but differed in their details, reflecting differences in local conditions.

TABLE 2

Summary of the parameters of the local base series of models in sections KG1-KG10

Parameter		KG1	KG2	KG3	KG4	KG5	KG6	KG7	KG8	KG9	KG10
Arch spacing [m]		—	1.0	0.5	0.5	0.5	0.5	—	1.0	0.75	0.75
Bedding plane dip angle [°]		21.6	27.6	25.3	31.8	17.4	26	22	22.4	22	17
Bedding plane dip azimuth [°]		84.1	65.2	44.2	24.2	13.3	72	65	39.7	30	10
Ubiquitous joints	Weakness plane, dip angle [°]	21.6	27.6	25.3	31.8	17.4	26	22	22.4	22	17
	Weakness plane, dip direction [°]	84.1	65.2	44.2	24.2	13.3	72	65	39.7	30	10
	Cohesion [MPa]	0.082	0.055	0.114	0.103	0.056	0.045	0.044	0.04	0.05	0.052
	Friction angle [°]	22.09	17.81	27.1	25.42	18.04	16.07	15.95	15.32	16.9	17.38
	Dilation angle [°]	11.47	9.13	14.35	13.37	9.25	8.2	8.13	7.8	8.64	8.89
	Tensile strength [MPa]	0.038	0.024	0.056	0.05	0.025	0.018	0.018	0.016	0.021	0.023

TABLE 3

Summary of the parameters of the local base series of models common to all the sections

Parameter		KG1-KG10
Equivalent spacing of the main discontinuity [m]		0.724
Rock material	Density of the material [Mg/m^3].	2.2
	Young's modulus [MPa]	2250
	Cohesion [MPa]/Friction angle [°]/Dilatancy angle [°]	0.135/30/16.1
	Tensile strength [MPa]	0.0675
Bedding plane discontinuity	Kn/Ks [MPa/m]	2000/1000
	Cohesion [MPa]/Friction angle [°]/Dilatancy angle [°]	0.011/10.2/5.16
	Tensile strength [MPa]	0
Joint discontinuity	Kn/Ks [MPa/m]	4200/2100
	Cohesion [MPa]/Friction angle [°]/Dilatancy angle [°]	0.015/30/16.1
	Tensile strength [MPa]	0
Shotcrete	Thickness [m]	0.2
	Modulus of elasticity of concrete [MPa].	23,000
	Kn/Ks [MPa/m] between shotcrete and rock	10,000/2000
	Tensile strength [MPa]	1
	Cohesion [MPa]/Friction angle [°] between concrete and rock	0.50/60
Arches (supporting structural elements)	Modulus of elasticity of the arch [MPa].	23,000
	Cohesion [MPa]/Friction angle [°] between arches and rocks	0.50/60
	Kn/Ks between arches and rock [MPa/m]	1000/1000
	Tensile strength [MPa]	550
Rock bolts	Length [m]/spacing [m]	3/1
	Breaking strength	0.118
	Axial stiffness [MPa/m]	306

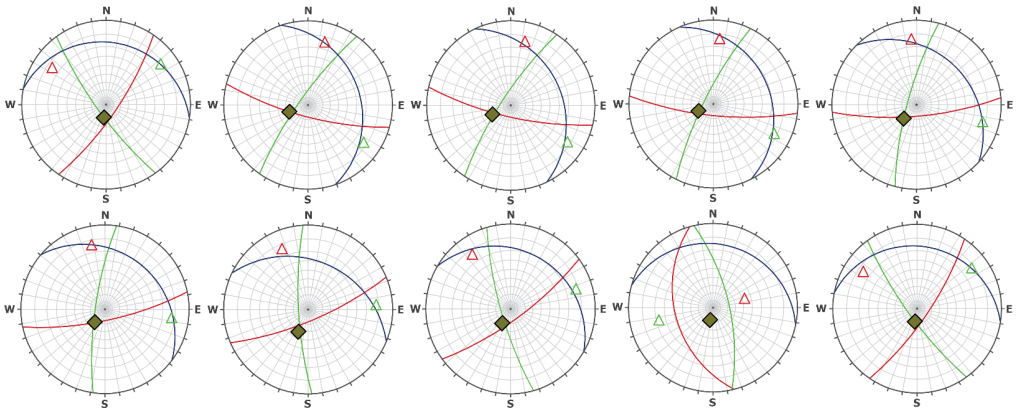

Fig. 6. Orientation of bedding and two joint sets for local models KG1-KG10 in local coordinate systems. Lower hemisphere equal angle projections. The local tunnel axis plunge/trend is 0°/0°

5.2. Simulation results for the base series

Geomechanical simulations of the behaviour of the flysch rock mass at ten different locations (KG1-KG10) were conducted. The roof displacement (u_{roof}), surface displacement (u_{sur}), and convergences (k_1, k_2, k_3) were obtained. The results and their mean absolute error (MAE) concerning the in situ measurements are presented in TABLE 4. These values are the major results and the starting point for further analysis.

Figs. 7 and 8 show the displacement distributions around the tunnel. Notably, as in the actual tunnel, the models of the sections differ in terms of the loading, orientation and density of discontinuities, rock properties, and support. The simulation results reveal a variation in the response of the rock mass across the ten cross-sections. The asymmetries in the displacements and forces around the tunnel are related to the influence of the orientation of the discontinuities on the displacement of the rock mass around the tunnel. A hypothetical tunnel collapse without support was also simulated for one of the tunnel cross-sections, as shown in Fig. 9.

TABLE 4

Simulation results and mean absolute errors for the KG1-KG10 base series. Negative values of displacement and convergence indicate subsidence and distance reduction, respectively

	KG1	KG2	KG3	KG4	KG5	KG6	KG7	KG8	KG9	KG10	Mean KG1-KG10
u_{roof} [mm]	−4.34	−4.87	−8.05	−5.15	−11.19	−8.8	−12.33	−8.33	−6.75	−4.47	−7.43
u_{sur} [mm]	−6.29	−6.03	−8.65	−6.98	−12.4	−10.79	−13.78	−8.12	−9.58	−5.8	−8.84
k_1 [mm]	−11.44	−9.37	−12.06	−9.04	−18.67	−11.13	−17.48	−7.05	−16.09	−8.66	−12.1
k_2 [mm]	−4.19	−3.41	−5.2	−3.97	−7.97	−4.14	−7.31	−3.42	−4.65	−3.21	−4.75
k_3 [mm]	−4.39	−3.73	−4.31	−1.86	−5.67	−2.93	−4.77	−2.81	−4.86	−2.81	−3.81
MAE [mm]	3.33	2.81	2.89	2.82	2.00	1.22	3.57	3.61	1.56	3.81	2.76

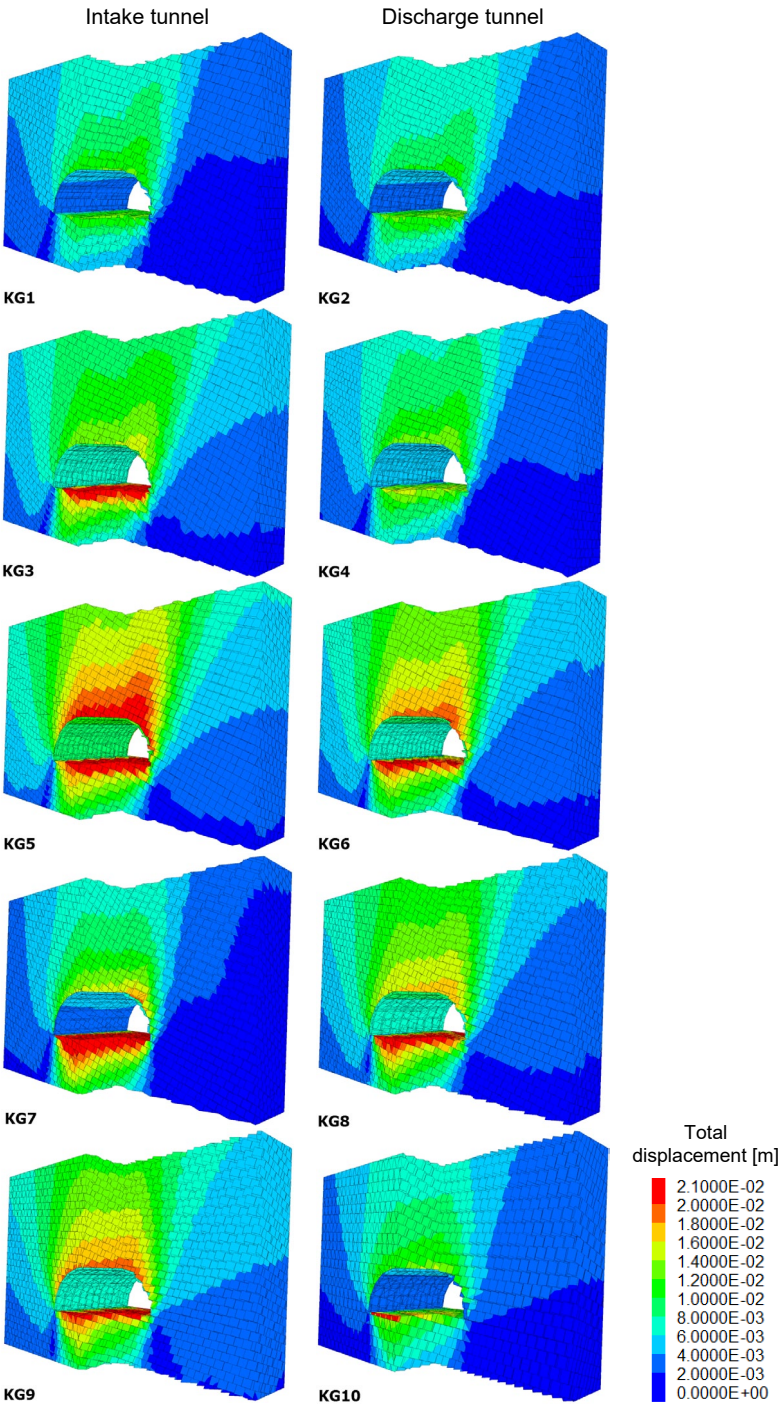

Fig. 7. Total displacement

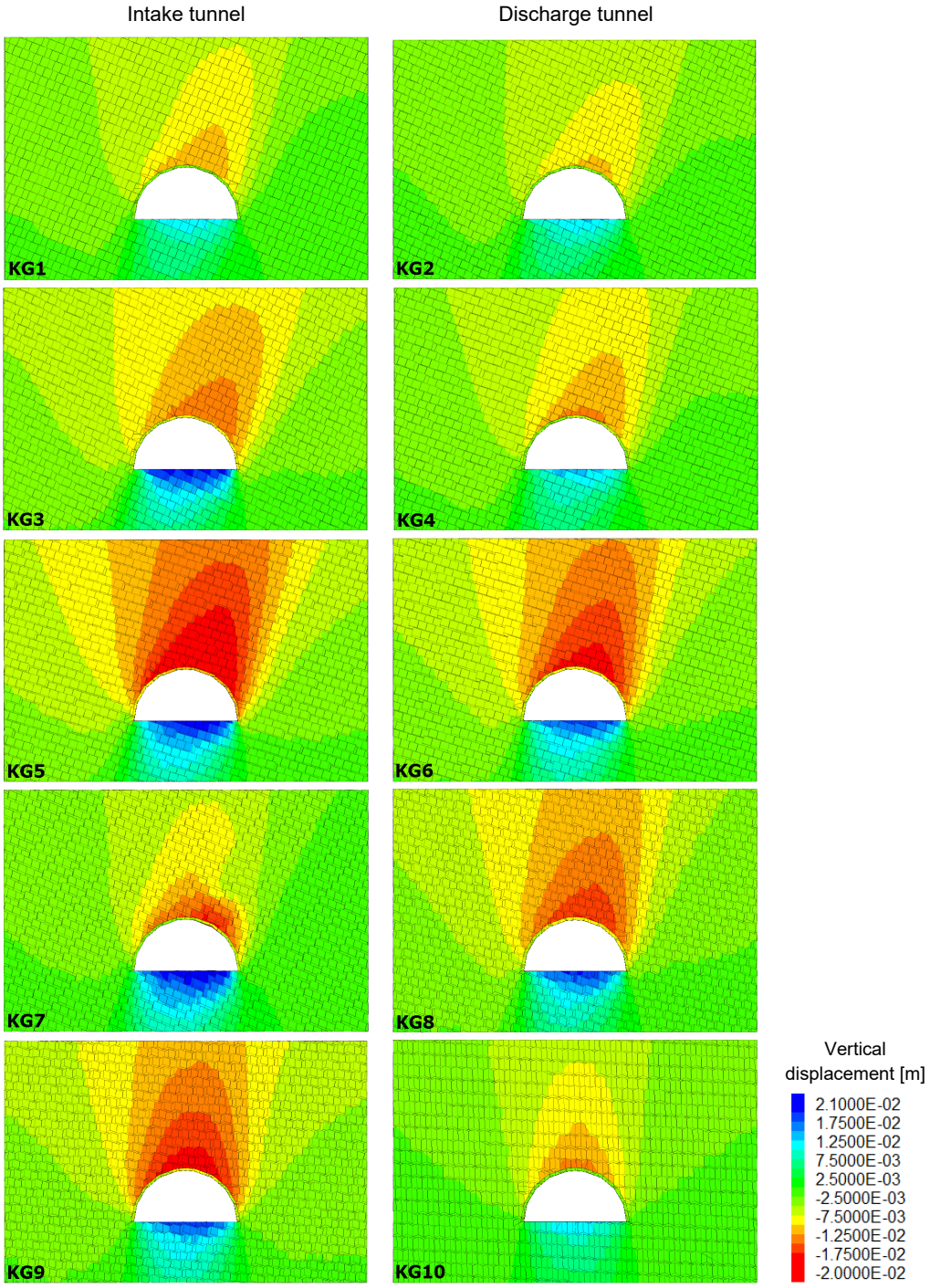

Fig. 8. Vertical displacement

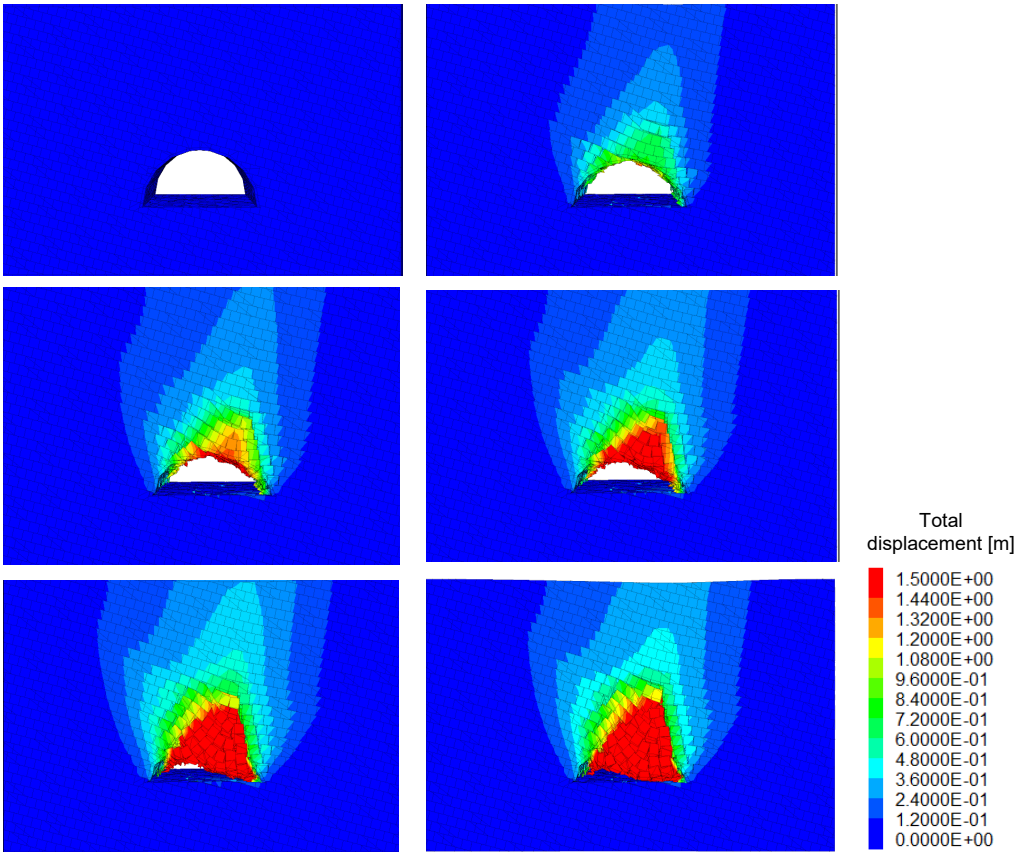

Fig. 9. Visualisation of the tunnel collapse in the KG6 cross-section. Displacement distribution in subsequent simulation steps

5.3. Preliminary examination of the model

Numerical simulations of rock mass behaviour are based on component mathematical and physical models of rock mass material and structural phenomena and multiple parameter values derived from studies and experiments. Because of the complexity of this system, the model response to these parameters is complex. The preliminary examination reveals these dependencies at the lowest possible computational cost.

To this end, the properties of the numerical model for the KG6 cross-section were investigated and subjected to simulation experiments. Five factors were investigated at two or three levels: WSkal is the strength of the rock (two levels), ESkal is the elastic modulus of the rock (three levels), WNiec is the strength of the bedding plane discontinuity (three levels), IDylat is the quotient of the tangent of the dilatancy angle and tangent of the friction angle (two levels), and KnKs is the normal and tangential stiffnesses of discontinuities (two levels). The experiments were conducted according to a mixed D-optimal design (24 runs, D-optimality 0.82). The model parameters are listed in TABLE 5.

TABLE 5

Examination of a model. Factors and parameters of the numerical experiments

Factors	Model parameters		Level		
			–1	0	1
WSkal: strength of rock	Friction angle [°]		18.9	—	26.7
	Cohesion [MPa]		0.049	—	0.072
	Tensile strength [MPa]		0.019	—	0.028
ESkal: rock stiffness	Young's modulus [MPa]		1500	2250	3000
WNiec: strength of discontinuities	Friction angle [°]		10.2	14.0	17.6
	Cohesion [MPa]		0.011	0.015	0.019
	Tensile strength [MPa]		0	0	0
IDylat: dilatancy factor	Quotient of the tangents of the dilation angle and friction angle		0	—	0.50
KnKs: stiffness of discontinuities	Bedding planes	normal stiffness [MPa/m]	1000	—	3000
		tangential stiffness [MPa/m]	500	—	1500
	Joints	normal stiffness [MPa/m]	2100	—	6300
		tangential stiffness [MPa/m]	1050	—	3150

The MAEs of the simulations were assessed by comparing the measured and calculated convergences and displacements of the geodetic benchmarks.

The main effect and interaction analyses were performed using a linear model with two-factor interactions. Fig. 10 shows the experimentally obtained marginal means of the simulation error with 95% confidence limits for the five tested factors.

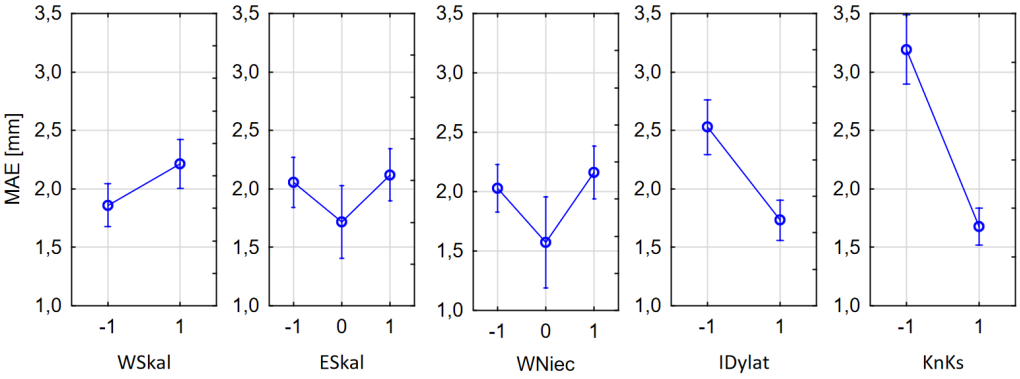

Fig. 10. Results of the experiment MAE marginal means for the five factors studied

In the subsequent steps, statistically nonsignificant effects were eliminated from the response model. The results of the effect analysis are shown in the Pareto chart in Fig. 11. The discontinuity stiffness and dilatancy significantly affect the simulation error either directly or through interactions. The physical interpretations of these parameters are complex, and laboratory or analytical evaluations are ambiguous; therefore, these parameters rarely attract attention when numerical simulations are being conducted or interpreted.

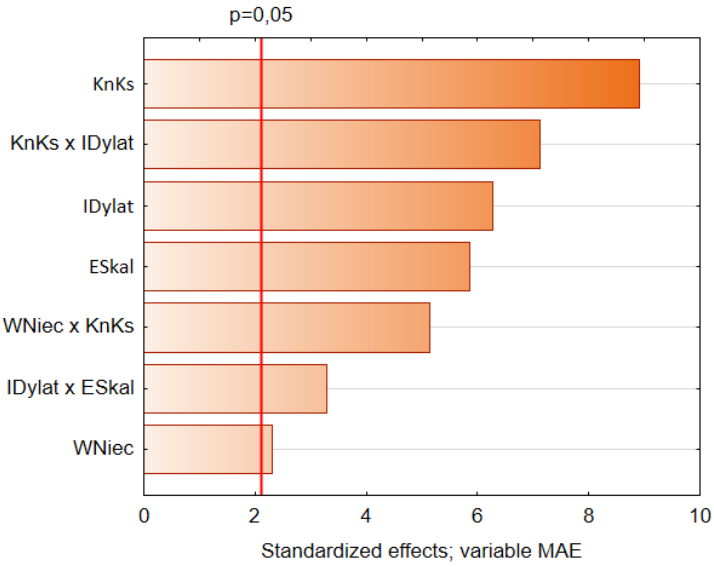

Fig. 11. Pareto chart of effects. Relevant linear main effects and first-order interactions

5.4. Model calibration and validation

Uncertainty exists in the estimation of rock mass parameter values and their spatial variability; therefore, the model parameters were calibrated on the basis of actual deformation measurements. Calibration represents a final fine-tuning of the model via available measurement data rather than a process of selecting parameter values from among all theoretically possible values.

After an initial set of model parameters from existing studies and documentation was adopted, several modified sets of parameters were tested, and the best set was selected. Calibration was conducted via simulations on five cross-sections (KG1, KG2, KG7, KG9, and KG10) representing different local conditions. The measurements were taken as reference values for the observed roof and surface displacements, as well as for the horizontal and sidewall convergences. The objective function was the MAE of the five observed displacement and convergence values in the five tunnel cross-sections. The calibration plan, which includes 12 calibration series, is listed in TABLE 6. The results are presented in TABLE 6. The smallest value of the objective function was obtained for the base series and the corresponding dataset. However, the calibration identified the best model and was an important component of the proposed methodology.

The model was validated by comparing the simulation results with the actual in situ values. The measurements at the cross-sections KG3, KG4, KG5, KG6, and KG8, which were not corrected in the data cleaning process or used in the calibration process, were used for validation. A comparison of the simulation and measurement results for five cross-sections of the discharge and intake tunnels under different local conditions revealed that the average absolute error for the cross-sections varies from 1.22 mm to 3.61 mm and averages 2.51 mm (TABLE 7). This value was deemed to be better than the acceptable value; thus, the models were successfully validated.

Given the complexity of the mechanics of flysch rock masses, the uncertainty of the model parameters, the approximate nature of the models of physical phenomena, the numerical errors,

TABLE 6

Calibration plan and simulation errors for all simulations performed to calibrate the model in the cross-sections KG1, KG2, KG7, KG9, and KG10

Series		Short description	MAE [mm]
0	Base	Parameter values adopted based on information on the properties of the rock mass around the tunnels and the simulation methodology.	3.02
1	WNiec1	Modification of the strength properties of the bedding plane discontinuities Equivalent material properties unchanged.	3.89
2	WNiec2	Modification of the strength properties of the bedding plane discontinuities. Equivalent material properties modified accordingly.	3.93
3	ESkal1	Modification of modulus of elasticity of rock, variant 1	3.68
4	Dylat1	Modification of dilation angle	3.43
5	ESkał2	Modification of modulus of elasticity of rock, variant 2	4.28
6	KnKs1	Modification of tangential and normal stiffness of discontinuities, variant 1	4.06
7	KnKs2	Modification of tangential and normal stiffness of discontinuities, variant 2	3.44
8	KnKs3	Modification of tangential and normal stiffness of discontinuities, variant 3	3.97
9	WSkal1	Modification of rock equivalent properties, variant 1	3.40
10	WSkal2	Modification of rock equivalent properties, variant 2	3.54
11	WSkal3	Modification of rock equivalent properties, variant 3	3.81
12	WSkal4	Modification of rock equivalent properties, variant 4	3.35

TABLE 7

Summary of the validation results. Deformations and mean absolute error

Cross-Section	u_{roof} [mm]	u_{sur} [mm]	k_1 [mm]	k_2 [mm]	k_3 [mm]	MAE [mm]
KG3	−8.05	−8.65	−12.06	−5.20	−4.31	2.89
KG4	−5.15	−6.98	−9.04	−3.97	−1.86	2.82
KG5	−11.19	−12.40	−18.67	−7.97	−5.67	2.00
KG6	−8.80	−10.79	−11.13	−4.14	−2.93	1.22
KG8	−8.33	−8.12	−7.05	−3.42	−2.81	3.61
Mean	−8.30	−9.39	−11.59	−4.94	−3.51	2.51

and the uncertainty of the measurement data, significantly large differences could be expected between the simulation and measurement results.

5.5. Sources of results uncertainty

Two sources of model-induced uncertainty were considered: the effect of continuous domain discretisation and the effect of the discontinuous displacement field along the tunnel axis.

For similar models differing in the generated discretisation mesh model, the results can differ, even if the general properties of the mesh are the same. For discrete models, this problem is related to the discretisation of the deformable blocks. To estimate the effect of the 3DEC finite-difference mesh on the simulation results, simulations were performed for five randomly generated meshes. The impact of the different meshes was estimated concerning the average deformation

values from the five simulations and not in comparison to in situ deformation measurements. The mean absolute deviation (MAD) in the estimation of the uncertainty of the simulation derived from this source is 0.7 mm.

The second considered source is the effect of the discontinuous displacement field along the tunnel axis.

The same 3D local model of a flysch rock mass may yield different displacement values, depending on the position of the benchmark in the model along its axis relative to the locations of the surrounding discontinuities. To investigate the respective uncertainties, displacements and convergences were investigated with two models (KG3 and KG6), each with five cross-sections. The simulation error was estimated using the MAD relative to the average values of the five simulations. The mean value of the MADs from models KG3 and KG6 is equal to 0.5 mm and can be considered an assessment of the uncertainty emerging from this source.

6. Parametric analysis

Once the model is validated, it can be used for design purposes. The application of the model to a variant simulation of a tunnel under a horizontal ground surface was demonstrated using the tunnel orientation, geometry, size, type of support (shotcrete, rock bolts, and steel arches), and rock mass properties of the KG6 model. The factors investigated were tunnel depth, bedding plane dip, bedding plane dip direction, and arch support density. The values of these factors for the experimental design are presented in TABLE 8.

TABLE 8

Scheme of the experiment conducted by varying one factor at a time;
the values of the factors tested

Simulation	Depth [m]	Bedding plane dip direction [°]	Bedding plane dip angle [°]	Number of steel arches per 1 m
A3, B3, C3, D3	60	45	40	1
A1	20	45	40	1
A2	40	45	40	1
A4	80	45	40	1
A5	100	45	40	1
B1	60	0.0	40	1
B2	60	22.5	40	1
B4	60	67.5	40	1
B5	60	90.0	40	1
C1	60	45	0	1
C2	60	45	20	1
C4	60	45	60	1
C5	60	45	80	1
D1	60	45	40	0.0
D2	60	45	40	0.5
D4	60	45	40	1.5
D5	60	45	40	2.0

The tunnel axis plunge/trend is 0°/0° in all cases, and the considered local bedding orientation is relative to the tunnel axis. The study was conducted by changing one factor at a time. This design easily reveals the existing relationships; however, it does not consider their interactions. The parameters not being tested are the same as those for the base series model KG6.

Fig. 12 shows the effects of the four factors on the displacements and convergences of the excavation. The left axes show the displacements of the roof, the surface above the measurement section, and the average convergence of the sidewalls (k23), whereas the right axes show horizontal convergence (k1).

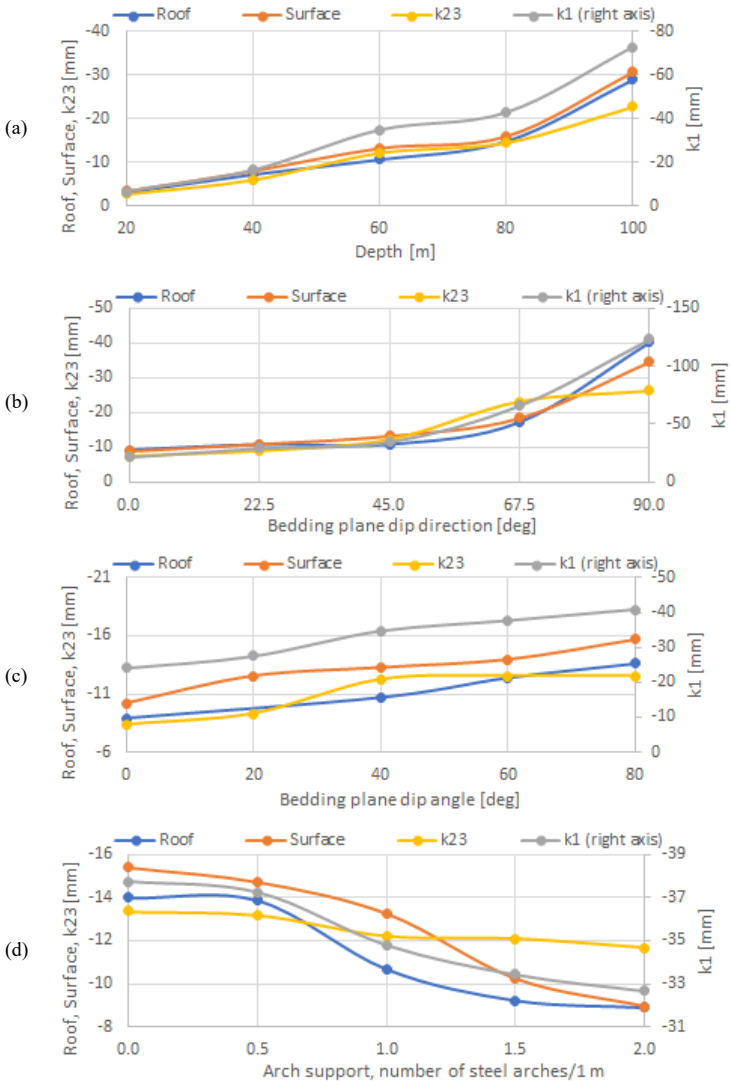

Fig. 12. Displacements and convergence as a function of (a) depth, (b) bedding plane dip direction, (c) bedding plane dip angle, and (d) density of arch support

Fig. 12a shows a significant increase in all displacements and convergences with increasing depth within the range of 20-100 m. The effect of depth is approximately linear for all deformations. The horizontal convergence has the highest maximum value because of the structure of the support, which lacks invert and is open at the bottom.

Fig. 12b shows the significant effect of the bedding plane dip direction on the deformation. The dip direction in the local coordinate system was investigated in the range from 0° (the bedding strike is perpendicular to the tunnel axis) to 90° (the bedding strike is parallel to the tunnel axis). Notably, all the displacements and convergences are the smallest for a bedding plane dip direction of 0° and increase slightly until a bedding plane dip direction of approximately 45°. Furthermore, except for the increase in the average convergence of the sidewalls (k23), the increases in the displacements and convergences accelerate to 90°.

Fig. 12c shows the dependence of the observed deformations on the dip angle of the bedding with a dip direction of 45°. All the observed deformations were greater for a dip angle of 80° than for a horizontal bedding (dip angle of 0°).

Steel arches, along with rock bolts and shotcrete, were components of the support system for this tunnel. Fig. 12d shows displacements as functions of the density of arches in the range of 0-2 arches/m at a depth of 60 m and a bedding plane dip angle of 40°. With increasing arch density and stiffness of the steel support, all the convergences and displacements decreased. The effect of the arch support was the smallest on the convergence of the sidewall and the largest on the surface and roof displacements.

Fig. 13 shows the convergence asymmetry, as measured by the difference in the convergence of the left and right sidewalls (k2-k3). This asymmetry is most greatly influenced by the dip direction of the discontinuity, with the convergence asymmetry being positive or negative, depending on its value. This effect is related to the complex mechanism of the interaction between the sup-

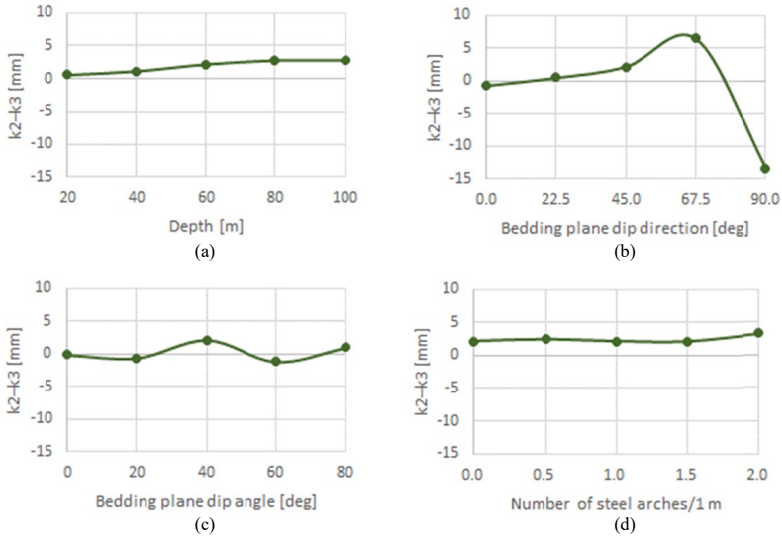

Fig. 13. Convergence asymmetry (difference between the convergences of the left and right sidewalls) as a function of (a) depth, (b) bedding plane dip direction, (c) bedding plane dip angle, and (d) density of arch support

port system without an invert and the layered rock mass. The influences of other factors on the convergence asymmetry are negligible or within the error of the simulation. However, the effect of the bedding dip angle on convergence asymmetry is dependent on the orientation of the bedding relative to the tunnel axis. For a dip direction of 45° (Fig. 13c), this influence is negligible.

7. Discussion

The proposed flysch rock mass model combines the characteristics of a blocky structure and a dense network of discontinuities. For a flysch rock mass with dense bedding, its discontinuous character is represented by small discrete blocks and the ubiquitous joint material within the blocks. For a thick-layered flysch rock mass, the model represents the natural structures of large blocks and the behaviour of the rock material inside the blocks. The large spatial variability of the rock mass structure and properties of the flysch can be represented using different local models.

The simulation error relative to in situ deformation measurements was estimated to be small, indicating that the model can be used for quantitative, comparative and parametric analyses. However, quantitative results should be interpreted cautiously, as should any result of a rock mechanics simulation under complex geological conditions.

The validation of the model for Swinna Poreba was based on in situ deformation values assessed with the use of the ground surface, tunnel roofs, and sidewall survey benchmarks in five tunnel cross-sections. In other design situations, validation should be performed using other available measurement data or metrics.

Two parallel hydrotechnical tunnels were built in Swinna Poreba. A local model of the two tunnels, which was examined in the preliminary stage of our study, yielded results similar to those of single-tunnel models. Therefore, local models were built separately for each tunnel. The similarity between the results for a single tunnel and two tunnels may reflect site-specific features such as the considerable distance/diameter ratio, shallow location, asymmetric overburden loading, and bedding orientation. In general, a local model should include two tunnels and consider the stages of execution and mutual progress of the two adjacent tunnels.

The representation of the excavation cycle and delayed tunnel support is reflected in the model. However, the limited range of available reports on the progress of tunnel excavation and support installation enabled the process to be implemented in a similar manner in all the cross-sections, without differentiating between them.

The tunnels under consideration are located in weak flysch masses with dense bedding planes. The advantages of the methodology should be even more apparent in high-quality flysch rock masses, with a predominance of thick layers, or a significant variation in block sizes from extremely small to large.

The proposed methodology and models are deterministic. This approach appears to be adequate under the specific conditions. However, considering the increasing importance of reliability-based geotechnical design, an extension to a probabilistic approach might be considered.

8. Conclusions

This study presents an approach for numerically simulating the mechanical behaviour of a Carpathian flysch rock mass surrounding a tunnel. The proposed methodology employs the

DEM and 3DEC in a novel arrangement, enabling the representation of the behaviour of the rock mass within a wide range of structural models and properties of the Carpathian flysch. The models have reduced computational complexity and can be used in parametric multivariate analyses, which are particularly useful for the design and monitoring of tunnel construction. The model is a complex system with many hidden relations. Consequently, it is examined through numerical experiments designed with statistical methods. The methodology also incorporates uncertainty discussion, calibration, and model validation to improve the model, compare the results with actual values, and ultimately interpret the results correctly. For the studied hydrotechnical tunnels in Carpathian flysch, the simulation error relative to in situ displacements and convergences in five tunnel locations was shown to be small. However, discontinuity stiffness and dilatancy may substantially affect simulation error, yet these parameters are normally not explored when numerical simulations are being conducted or interpreted. The strong influence of bedding orientation relative to the tunnel axis on the deformation and asymmetry of sidewall convergence was demonstrated via parametric analysis. The observed displacements and convergences increased monotonically and nonlinearly with depth and decreased with increasing stiffness of the support arches.

References

[1] R. Hart, P.A. Cundall, J. Lemos, Formulation of a three-dimensional distinct element model – part II. Mechanical calculations for motion and interaction of a system composed of many polyhedral blocks. Int. J. Rock Mech. Min. Sci. Geomech. Abstr. **25**, 117-125 (1988). DOI: https://doi.org/10.1016/0148-9062(88)92294-2

[2] 3DEC 3-dimensional distinct element code. Itasca, Minneapolis, MN (2019).

[3] H. Konietzky, L. te Kamp, H. Hammer, S. Niedermeyer, Numerical modelling of in situ stress conditions as an aid in route selection for rail tunnels in complex geological formations in South Germany. Comput. Geotech. **28**, 495-516. DOI: https://doi.org/10.1016/S0266-352X(01)00009-X

[4] X. Wang, P.H.S.W. Kulatilake, W.D. Song, Stability investigations around a mine tunnel through three-dimensional discontinuum and continuum stress analyses. Tunn. Undergr. Space Technol. **32**, 98-112 (2012). DOI: https://doi.org/10.1016/j.tust.2012.06.003

[5] Z. Cui, D. Liu, F. Wu, Influence of dip directions on the main deformation region of layered rock around tunnels. Bull. Eng. Geol. Environ. **73**, 441-450 (2014). DOI: https://doi.org/10.1007/s10064-013-0511-6

[6] N. Esteban N, R. Galindo, A. Serrano, Analytical formulation for the deformability assessment of rock masses with filled discontinuities. Comput. Geotech. **136**, 104111 (2021). DOI: https://doi.org/10.1016/j.compgeo.2021.104111

[7] Z. Hu, B. Wu, N. Xu, K. Wang, Effects of discontinuities on stress redistribution and rock failure: a case of underground caverns. Tunn. Undergr. Space Technol. **127**, 104583 (2022). DOI: https://doi.org/10.1016/j.tust.2022.104583

[8] A. Shi, C. Li, W. Hong, G. Lu, J. Zhou, H. Li, Comparative analysis of deformation and failure mechanisms of underground powerhouses on the left and right banks of Baihetan hydropower station. J. Rock Mech. Geotech. Eng. **14**, 731-745 (2022). DOI: https://doi.org/10.1016/j.jrmge.2021.09.012

[9] W. Dong, S. Ji, C. Li, X. Chen, Y. Song, The influence of different influencing factors in the jointed rock formation on the failure mode of the tunnel. Geotech. Geol. Eng. **41**, 1183-1201 (2023). DOI: https://doi.org/10.1007/s10706-022-02329-w

[10] H. Fan, L. Li, P. Zong, H. Liu, L. Yang, J. Wang, P. Yan, S. Sun, Advanced stability analysis method for the tunnel face in jointed rock mass based on DFN-DEM. Undergr. Space. **13**, 136-149 (2023). DOI: https://doi.org/10.1016/j.undsp.2023.03.009

[11] T.A. Phan, Modelling of flysch rock mass behavior in tunnel vicinity with discrete blocks approach. PhD Thesis, AGH University of Krakow, Poland (2023).

[12] Y. Chen, J. Teng, 3DEC numerical analysis of failure characteristics for tunnel in stratified rock masses. KSCE J. Civ. Eng. **28**, 2420-2426 (2024). DOI: https://doi.org/10.1007/s12205-024-1318-7

[13] N. Xu, J. Zhang, H. Tian, G. Mei, Q. Ge, Discrete element modeling of strata and surface movement induced by mining under open-pit final slope. Int. J. Rock Mech. Min. Sci. **88**, 61-76, (2016). DOI: https://doi.org/10.1016/j.ijrmms.2016.07.006.

[14] B. Regassa, N. Xu, G. Mei, An equivalent discontinuous modeling method of jointed rock masses for DEM simulation of mining-induced rock movements. Int. J. Rock Mech. Min. Sci. **108**, 1-14 (2018). DOI: https://doi.org/10.1016/j.ijrmms.2018.04.053

[15] D. Donati, D. Stead, T.W. Stewart, J. Marsh, Numerical modelling of slope damage in large, slowly moving rockslides: insights from the downie slide, British Columbia, Canada. Eng. Geol. **273**, 105693 (2020). DOI: https://doi.org/10.1016/j.enggeo.2020.105693

[16] H. Wang, B. Zhang, G. Mei, N. Xu, A statistics-based discrete element modeling method coupled with the strength reduction method for the stability analysis of jointed rock slopes. Eng. Geol. **264**, 105247 (2020). DOI: https://doi.org/10.1016/j.enggeo.2019.105247

[17] L. Zabuski, G. Marcato, Analysis of potential landslide processes in the Passo della Morte (Carnian Alps, Italy). Geol. Q. **64**, 681-691 (2020). DOI: https://doi.org/10.7306/gq.1552

[18] B. Liu, K. He, M. Han, X. Hu, T. Wu, M. Wu, G. Ma, Dynamic process simulation of the Xiaogangjian rockslide occurred in shattered mountain based on 3DEC and DFN. Comput Geotech **134**, 104122 (2021). DOI: https://doi.org/10.1016/j.compgeo.2021.104122

[19] J.H. Wu, P.H. Hsieh, Simulating the postfailure behavior of the seismically- triggered Chiu-Fen-Erh-Shan landslide using 3DEC. Eng. Geol. **287**, 106113 (2021). DOI: https://doi.org/10.1016/j.enggeo.2021.106113

[20] A.S. Mreyen, D. Donati, D. Elmo, F.V. Donze, H.B. Havenith, Dynamic numerical modelling of co-seismic landslides using the 3D distinct element method: insights from the Balta rockslide (Romania). Eng. Geol. **307**, 106774 (2022). DOI: https://doi.org/10.1016/j.enggeo.2022.106774

[21] P.H.S.W. Kulatilake, Q. Wu, Z. Yu, F. Jiang, Investigation of stability of a tunnel in a deep coal mine in China. Int. J. Min. Sci. Technol. **23**, 579-589 (2013). DOI: https://doi.org/10.1016/j.ijmst.2013.07.018

[22] S.Q. Yang, M. Chen, H.W. Jing, K.F. Chen, B. Meng, A case study on large deformation failure mechanism of deep soft rock roadway in Xin'An coal mine, China. Eng. Geol. **217**, 89-101 (2017). DOI: https://doi.org/10.1016/j.enggeo.2016.12.012

[23] Y. Xing, P.H.S.W. Kulatilake, L.A. Sandbak, Effect of rock mass and discontinuity mechanical properties and delayed rock supporting on tunnel stability in an underground mine. Eng. Geol. **238**, 62-75 (2018). DOI: https://doi.org/10.1016/j.enggeo.2018.03.010

[24] A. Li, F. Dai, N. Xu, G. Gu, Z. Hu, Analysis of a complex flexural toppling failure of large underground caverns in layered rock masses. Rock Mech. Rock Eng. **52**, 3157-3181 (2019). DOI: https://doi.org/10.1007/s00603-019-01760-5

[25] T.D. Le, J. Oh, Longwall face stability analysis from a discontinuum-discrete fracture network modelling. Tunn. Undergr. Space Technol. **124**, 104480 (2022). DOI: https://doi.org/10.1016/j.tust.2022.104480

[26] F. Wang, D. Shao, C. Zhang, Z. Song, Overlying sand-inrushing mechanism and associated control technology for longwall mining in shallow buried coal seams with the soft surrounding rock. Arch. Min. Sci. **67**, 4, 681-697 (2022). DOI: https://doi.org/10.24425/ams.2022.143681

[27] J. Jakubowski, 3DEC modeling results generalized by stochastic approach. In: Proceedings of the first international UDEC/3DEC symposium: numerical modeling of discrete materials in geotechnical engineering, civil engineering, and earth sciences, Bochum, Germany. Taylor & Francis Group, London, UK, p. 165-174 (2004).

[28] J. Jakubowski, A. Tajduś, The 3D Monte-Carlo simulation of rigid blocks around a tunnel. In: Mechanics of jointed and faulted rock, proceedings of the 2nd international conference, Vienna, Austria. A. A. Balkema, London, UK, p. 551-556 (1995).

[29] J. Jakubowski, Probabilistic stability analysis of a tunnel in a fracture zone. Arch. Min. Sci. **56**, 405-413 (2011).

[30] J. Jakubowski, The stochastic block stability simulation method and other probabilistic extensions of block theory. Arch. Min. Sci. **56**, 223-238 (2011).

[31] J. Sjöberg, L. Malmgren, Application of global-local modelling to mining rock mechanics problems. In: Proceedings of the first international FLAC/DEM symposium on numerical modeling. Minneapolis, Minn, p. 25-27 (2008).

[32] C. Edelbro, J. Sjöberg, L. Malmgren, C. Dahnér-Lindqvist, Prediction and follow-up of failure and fallouts in footwall drifts in the Kiirunavaara mine. Can. Geotech. J. **49**, 546-559 (2012). DOI: https://doi.org/10.1139/t2012-012

[33] H. Basarir H, Y. Sun, G. Li, Gateway stability analysis by global-local modeling approach. Int. J. Rock Mech. Min. Sci. **113**, 31-40 (2019). DOI: https://doi.org/10.1016/j.ijrmms.2018.11.010

[34] B. Zhao, X. Wang, C. Zhang, W. Li, R. Abbassi, K. Chen, Structural integrity assessment of shield tunnel crossing of a railway bridge using orthogonal experimental design. Eng. Fail. Anal. **114**, 104594 (2020). DOI: https://doi.org/10.1016/j.engfailanal.2020.104594

[35] A. Jiang, X. Guo, S. Zheng, M. Xu, Parameters identification of tunnel jointed surrounding rock based on Gaussian process regression optimized by difference evolution algorithm. Comput. Model. Eng. Sci. **127**, 1177-1199 (2021). DOI: https://doi.org/10.32604/cmes.2021.014199

[36] Y. Zhao, S.J. Feng, Back analysis of surrounding rock parameters of tunnel considering displacement loss and space effect. Bull. Eng. Geol. Environ. **80**, 5675-5692 (2021). DOI: https://doi.org/10.1007/s10064-021-02254-x

[37] M. Schoen, R. Hölter, D. Boldini, A.A. Lavasan, Application of optimal experiment design method to detect the ideal sensor positions: a case study of Milan metro line 5. Tunn. Undergr. Space Technol. **130**, 104723 (2022). DOI: https://doi.org/10.1016/j.tust.2022.104723

[38] Y. Wu, H. Wang, X. Guo, Inversion of surrounding red-bed soft rock mechanical parameters based on the PSO-XGBoost algorithm for tunnelling operation. Appl. Sci. **13**, 13341 (2023). DOI: https://doi.org/10.3390/app132413341

[39] J. Cui, S. Wu, H. Cheng, G. Kui, H. Zhang, M. Hu, P. He, Composite interpretability optimization ensemble learning inversion surrounding rock mechanical parameters and support optimization in soft rock tunnels. Comput. Geotech. **165**, 105877 (2024). DOI: https://doi.org/10.1016/j.compgeo.2023.105877

[40] X. Zhang, D. Zhang, Y. Rong, Y. Ma, C. Yao, Y. Sun, Study on the stability of tunnel in weak surrounding rock considering initial support parameters and excavation method. KSCE J. Civ. Eng. **28**, 2427-2439 (2024). DOI: https://doi.org/10.1007/s12205-024-1520-7

[41] Z. Bestyński, K. Thiel, L. Zabuski, Geotechnical classifications of flysch rock mass. Hydrotech. Diss. 52. (1991)

[42] K. Thiel, Physico-mechanical properties and models of the polish flysch carpathians rock mass. Archives of Hydro-Engineering and Environmental Mechanics, Gdańsk, Poland (1995).

[43] L. Zabuski, Behavior of the flysch rock environment surrounding the tunnel. Archives of Hydro-Engineering and Environmental Mechanics, Gdańsk, Poland (2002).

[44] M. Dynowska, Prediction of the deformation of the flysch rock mass in the tunnel surroundings. Ph.D. Thesis, AGH University of Science and Technology, Kraków, Poland (1999).

[45] J. Pinińska, Geological and engineering evaluation systems for rocks and rock masses. Przegląd Geologiczny **49**, 804-814 (2001).

[46] P. Marinos, E. Hoek, Estimating the geotechnical properties of heterogeneous rock masses such as flysch. Bull. Eng. Geol. Environ. **60**, 85-92 (2001). DOI: https://doi.org/10.1007/s100640000090

[47] Z. Pilecki, Geotechnical model of rock mass for road tunnel projection in the Carpathian flysch. Publications of the Institute of Geophysics, Polish Academy of Sciences, Series M: Miscellanea. **24**, 383-396 (2002).

[48] P. Łukaszewski, Assessment of Flysch sandstones' strength at various loading paths in conditions of conventional triaxial compression. Przegląd Geologiczny **53**, 596-601 (2005).

[49] T. Majcherczyk, Z. Pilecki, Z. Niedbalski, E. Pilecka, M. Blajer, J. Pszonka, The influence of geological engineering and geotechnical conditions on parameter selection of the primary lining of a road tunnel in Laliki. Miner. Resour. Manag. **28**, 103-124 (2012). DOI: https://doi.org/10.2478/v10269-012-0006-2

[50] J.P. Kogut, E. Pilecka, D. Szwarkowski, Analysis of landslide effects along a road located in the Carpathian flysch. Open Geosciences **10** (1), 517-531 (2018).

[51] Z. Niedbalski, P. Małkowski, T. Majcherczyk, Application of the NATM method in the road tunneling works in difficult geological conditions – the Carpathian flysch. Tunn. Undergr. Space Technol. **74**, 41-59 (2018). DOI: https://doi.org/10.1016/j.tust.2018.01.003

[52] V. Marinos, A revised, geotechnical classification GSI system for tectonically disturbed heterogeneous rock masses, such as flysch. Bull. Eng. Geol. Environ. **78**, 899-912 (2019). DOI: https://doi.org/10.1007/s10064-017-1151-z

[53] V. Marinos, A. Goricki, E. Malandrakis, Determining the principles of tunnel support based on the engineering geological behaviour types: example of a tunnel in tectonically disturbed heterogeneous rock in Serbia. Bull. Eng. Geol. Environ. **78**, 2887-2902 (2019). DOI: https://doi.org/10.1007/s10064-018-1277-7

[54] M. Blajer, M. Cała, M. Kolano, A. Stopkowicz, A Tajduś, Identification of a flysch mass and classification of its quality. Mosty **3**, 89-92 (2019).

[55] B. Fleetwood, M.S. Brook, G. Brink, N.R. Richards, L. Adam, P.M. Black, Characterization of a highly heterogeneous flysch deposit and excavation implications: case study from Auckland, New Zealand. Bull. Eng. Geol. Environ. **79**, 4565-4578 (2020). DOI: https://doi.org/10.1007/s10064-020-01873-0

[56] A. Tajduś, K. Tajduś, Assessment of the behaviour of flysch rock mass during tunnel boring in the primary lining using indicators and limit values of displacements and deformations. Arch. Min. Sci. **67**, 2, 355-376 (2022). DOI: https://doi.org/10.24425/ams.2022.141463

[57] M. Blajer, Method of tunnel support design for Carpathian flysch conditions. PhD Thesis, AGH University of Science and Technology, Kraków, Poland (2023).